3D discrete kinematic modelling of sedimentary basin deformation

T. Cornu, F. Schneider and J. -P. Gratier

Geological Society, London, Special Publications 2003; v. 212; p. 275-283
doi:10.1144/GSL.SP.2003.212.01.18

3D discrete kinematic modelling of sedimentary basin deformation

T. CORNU[1], F. SCHNEIDER[1] & J.-P. GRATIER[2]

[1]*IFP, 1–4 avenue de Bois-Préau, 92500 Rueil-Malmaison, France (e-mail: tristan.cornu@ifp.fr; frederic.schneider@ifp.fr)*

Present address: Faculty of Earth and Life Sciences, Tectonics, Vrije Universiteit, De Boelelaan 1085, 1081 HV Amsterdam, The Netherlands (e-mail: tristan.cornu@falw.vu.nl)

[2]*LGIT, Observatoire de l'université de Grenoble, IRIGM, BP 53, 38041 Grenoble, France (e-mail: Jean-Pierre.Gratier@obs.ujf-grenoble.fr)*

Abstract: 3D coupled backward and forward deformation of geological layers is a new step in basin modelling. This problem can be treated with a mechanical or a kinematic approach. Because of the difficulties met with the mechanical approach, the kinematic approach is more often used. The kinematic model described here allows a geologically acceptable path to be built, which takes into account an incremental evolution of time. To obtain a better description of 3D geometries, the model uses a full hexaedric discretization. The discrete neutral surface of each layer is used to perform the flexural slip deformation.

The tectonic deformation of sedimentary rocks is one of the main problems in basin modelling (Schneider *et al.* 1996). In order to integrate tectonic deformation, including folds and faults, two approaches can be used: a mechanical approach, based on mechanical laws, or a kinematic approach, based on geometrical assumptions. The mechanical approach has given satisfying results for two-dimensional studies, and has been compared to experiments in a sandbox (Barnichon 1998) or applied to field cases (Hassani 1994; Niño *et al.* 1998). Nevertheless, a 3D mechanical model, which integrates all the relevant geological parameters, has not yet been proposed. The complexity of the phenomenon at the geological time and space scales, the lack of an adapted rheological law (Ramsay & Huber 1987; Lamoureux-Var 1997), and the difficulty of finding the right boundary conditions may explain this. The mechanical problem is a problem of large deformations and large displacements, so even a model like UDEC (Cundall 1988; Hart *et al.* 1988) has restrictive assumptions for applications to natural processes.

Because of the difficulties with the mechanical approach, an alternative is the kinematic approach. Such an approach is sufficiently representative of the natural processes. It can serve for future computations of transfer problems (thermic, fluids), evolution of rock attributes (porosity, permeability, thermal conductivity), and development of natural processes (sedimentation, erosion, compaction). To obtain a better description of the 3D geometries, the model proposed here is patterned after the 2D discrete approach developed by Diviès (1997). Such a discrete kinematic model allows one to build an acceptable geological path for backward and forward modelling. Unlike models of unfolding like UNFOLD (Gratier *et al.* 1991; Gratier & Guillier 1993) or PATCHWORK (Bennis *et al.* 1991), which unfold layers instantaneously, the new model uses an incremental evolution with time. Until now, most work on forward kinematic models has been performed in two dimensions (Suppe 1983; De Paor 1988*a*,*b*; Zoetemeijer 1992; Waltham 1989; Contreras 1990) based on the assumption of area conservation proposed by Dahlstrom (1969). However, some 2.5D models have been proposed from these 2D models (Wilkerson & Medwedeff 1991; Shaw *et al.* 1994; Egan *et al.* 1998). They extend the area conservation to volume conservation, but are limited to cylindrical cases, built from topologically equivalent 2D sections. The main restriction is that the associated finite displacement must be parallel in map view. Although these models allow the understanding of many cases, they cannot represent the complexity of a real three-dimensional case.

In the next section, we present a 3D model for kinematic deformation of a sedimentary basin. First, we explain the assumptions that sustain the

From: NIEUWLAND, D. A. (ed.) *New Insights into Structural Interpretation and Modelling*. Geological Society, London, Special Publications, **212**, 275–283. 0305-8719/03/$15

model, and how we express them in their mathematical form. Then we show the main results: (a) those in 2.5D that served to validate and to compare with existing model, (b) those in 3D to test the model on true tridimensional geometries. All the tests are performed for fault-bend-fold.

Principles of the model

The model proposed here can treat two mechanisms of deformation: vertical shear and flexural slip. We do not describe the equations of vertical shear, which are well known, but we propose a new model for the flexural slip mechanism. The modelling of the flexural slip is based on three main assumptions:

(1) the layers slip
(2) the thickness of each layer is preserved
(3) the area of the neutral surface of each layer is preserved.

Layer slip and preservation of thickness are the most often used assumptions in the literature (Suppe 1983; Waltham 1989, 1990), and they are relevant to the geological observations of the deformation of so-called competent layers (Ramsay & Huber 1987). The last assumption is more a mechanical one; it relies on the flexural mechanism and deals with the neutral surface of a layer, which is supposed to conserve its area through deformation (Ramsay & Huber 1987). Thus the motion of the neutral surface defines the motion of the layer. First the 2D model of the displacement of a neutral surface node is presented, then an extension to the 3D.

We now present the mathematical form of the model (Fig. 1a). In the 2D model, a polygonal line, cut by the bisectrix of each segment line angle, defines the basement of the basin. The layer is discretized with quadrilateral elements. For convenience, the neutral line is supposed to be the line that passes through the centre of the vertical edges.

Sliding support

The sliding support is defined with the bottom of the layer for the first layer of the hanging wall, and with the top of the previous layer for the upper layers. The support is then extended to the whole domain with the top of the other blocks. Each face of the layer is a draw segment, defined by equation:

$$\alpha x + \beta y + h = 0$$

where the coefficients α, β, and h are determined with the two points corresponding to the limits of the segment.

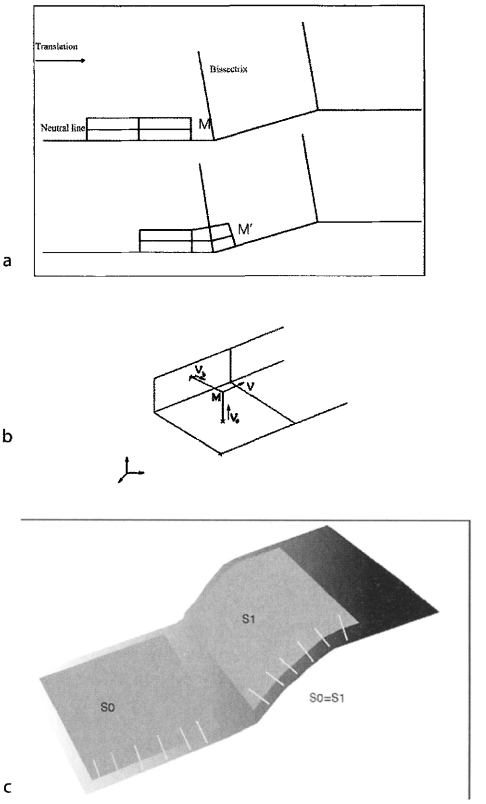

Fig. 1. (**a**) Diagram of the displacement of a node of the neutral line. (**b**) Definition of the displacement direction in 3D. (**c**) Diagram of the reconstruction of the vertical edges.

Bisectrix

As with Contreras & Suter's (1990) model, the sliding support is divided by the bisectrix of each intersecting segment. The coefficients of the bisectrix are determined by the definition of the segments pairs.

Curvilinear displacement

The displacement of the layer is achieved by the displacement of all the points of the neutral line. For M, a point of the neutral line, M' is the image point, by the transformation:

$$M' = \vec{t}_{\delta}\vec{v}\ (\mathbf{M})$$

where δ is the amount of displacement, and $\vec{v}$ the main direction.

Step of the displacement of a neutral line node

M_0 (x_0, y_0, z_0) is a node of the neutral line. Its displacement is parallel to the sliding support, and follows the draw D $(M, \vec{v}_h)$, where $\vec{v}_h$ is the orthogonal projection of $\vec{v}$ on the support:

$$D: \begin{cases} x_0 + v_{hx}t \\ y_0 + v_{hy}t \end{cases}$$

The point M_0 stay onto (D) until it intersects (D_b) one of the bisectrix of the support:

$$(D_b): \alpha_b x + \beta_b y + h_b = 0$$

The coordinates of $I = (D) \cap (D_b)$, intersection point of (D) and the bisectrix (D_b) are written:

$$I = \begin{cases} x_0 + v_{hx}t_{Ii} \\ y_0 + v_{hy}t_{Ii} \end{cases}$$

We deduced t_I with the following equation:

$$t_{Ii} = \frac{-(\alpha_b x_0 + \beta_b y_0 + h)}{\alpha_b v_{hx} + \beta_b v_{hy}}$$

We suppose $d = \|M_0 I\|$ to be the Euclidean distance between the two points I and M_0. The point M_0 has to displace of an amount of δ. We now have three possibilities:

1. $d > \delta$: the point M_0 has a displacement of δ along (D), and its new coordinates are:

$$M_0' = \begin{cases} x_0 + v_{hx}\delta \\ y_0 + v_{hy}\delta \end{cases}$$

2. $d = \delta$: the point M_0' is the same than point I.
3. $d < \delta$: M is displaced to I, but it still must displace a distance $\delta - d$. We repeat all the precedent operations, with initial point I and a new definition of $\vec{v}$ according to the sliding support.

Rebuild edges

The second step of the deformation is to rebuild the area of the layer. After translation of the neutral line, we have to rebuild the edges to restore the strained surface of the basin. The edges are rebuilt by a simple rigid rotation around the neutral line, whose area is preserved (Fig. 1c).

3D correction

The above equations are applied to the 2D cases, but they do not describe the lateral component of the displacement. Indeed, in 3D, we have to impose a new constraint on the displacement. The additional assumption we make in 3D is related to the conservation of the neutral lines, which is the lateral equivalent of the conservation of thickness: the width of the layer must be conserved. With this new assumption, the direction cannot be defined by a simple normal projection on the support. We define a laterally imposed surface, which allows the preservation of the neutral surface width (Fig. 1b).

The new direction $\vec{v}$ of the displacement is defined by:

$$\vec{v} = \vec{v}_s \, \Lambda \, \vec{v}_b$$

where $\vec{v}_s$ is the normal vector of the support, and $\vec{v}_b$ the normal vector of the lateral border (the imposed surface). Consequently the motion is parallel both to the basement of the layer and to the border we choose to impose as lateral reference.

Validation and results

The model was first validated in 2.5D and the results were compared to those of Wilkerson & Medwedeff's (1991) model. Similarly, we test the kinematic algorithm on two synthetic cases. The first test was made on a cylindrical basin, which is a succession of ten identical sections. It is 20 km long, 10 km wide, and 2 km thick (Fig. 2a). It is submitted to a displacement, which has a lateral variation that is defined by the relation for each time step:

$$\delta = 1000 \frac{(y_{\max} - y)}{y_{\max}}$$

The second test was made on an analytical basin, that has the same parameters as the first one, but instead of being cylindrical, it has a lateral variation of the strike of the ramp, from 10° to 25° (Fig. 2c). After displacement, 3 km for the first and 1 km for the second test, we observe good results for the deformation. We see similar shapes to those in Wilkerson & Medwedeff's model (Fig. 2b, d, e). We note a good geometric coherency, and the results obtained on a 60° fault confirm that we can handle more difficult geometries than the classical models, with strong dip for the ramp (Fig. 2f, g).

As the 2.5D results were satisfying, 3D tests have been performed on two similar cases. The purpose of these test cases is the validation on a 3D geometry, which is more complex than in 2.5D.

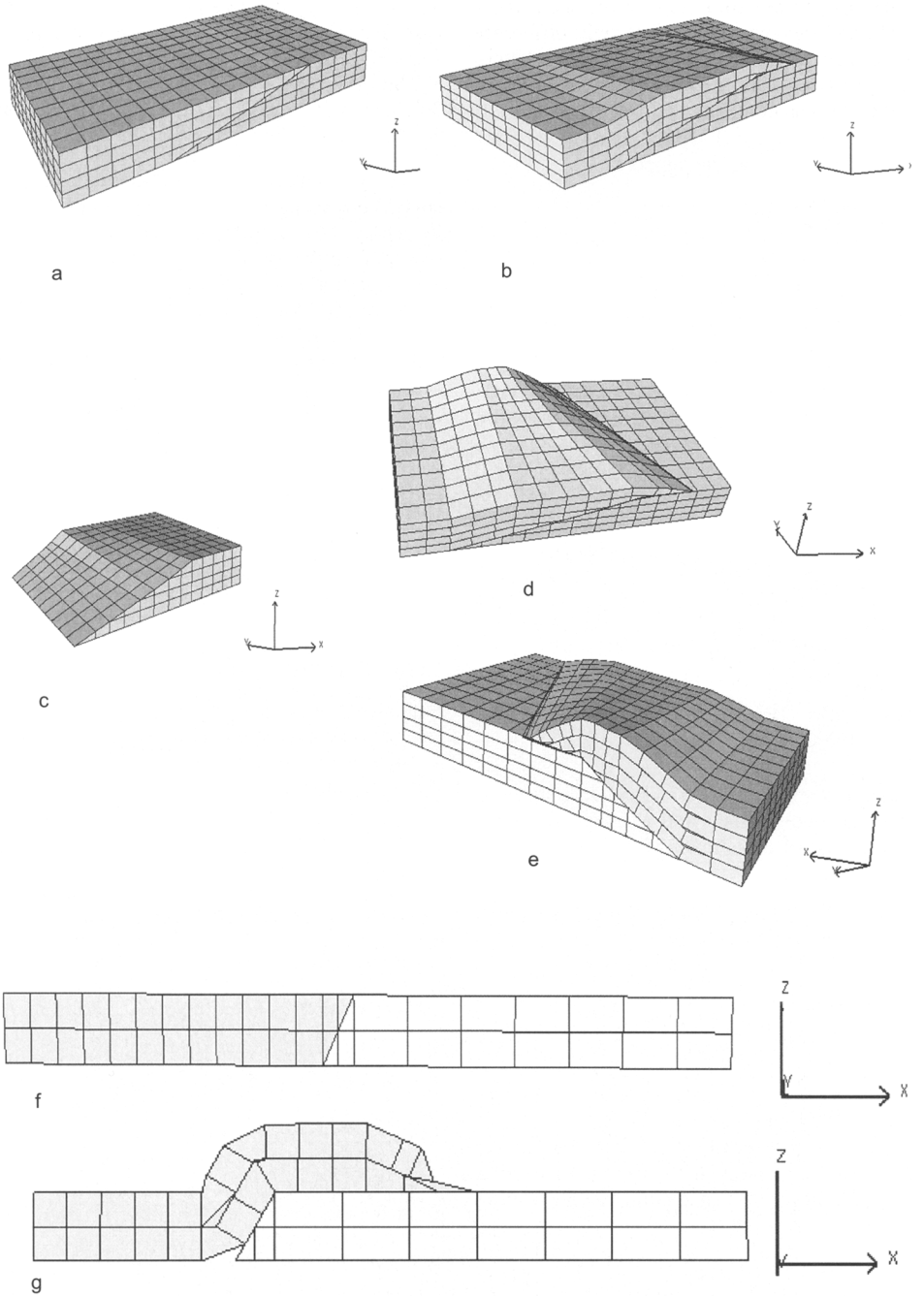

Fig. 2. 2.5D validation. (**a**, **b**) Initial and deformed configurations for a cylindrical block, deformed with shear displacement. (**c**, **d**, **e**) Initial and deformed configurations for a cylindrical block, with a variable ramp (from 10° to 25°). (**f**, **g**) Cross-sections for a basin with a 60° fault.

Two 3D cases were built both with the same hanging wall, and the same ramp. The only difference is the direction of the imposed surface that defines the 3D direction of the displacement. The first test case (Fig. 3a) has an imposed surface that is parallel to boundary displacement and the second test case (Fig. 4a) has an imposed surface that has a 5° angle with the boundary displacement.

The ramp of the basin is a curved ramp (Fig. 3b), with a 20° angle dip. The hanging wall at the

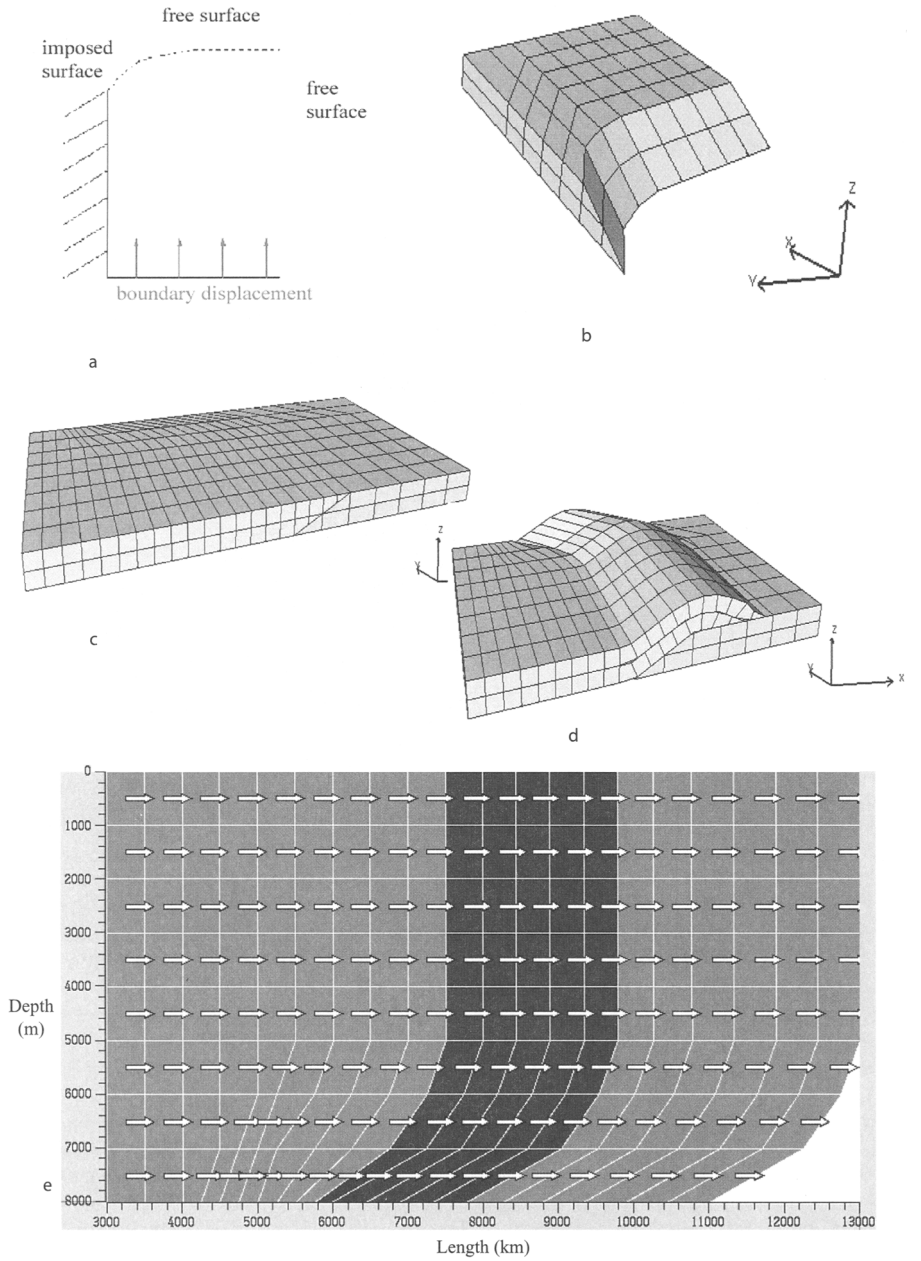

Fig. 3. First 3D validation test: lateral boundary parallel to the boundary displacement. (**a**) Diagram of the boundary conditions. (**b**) View of the curved ramp. (**c**) Initial state of the block. (**d**) Deformed configuration after 3000 m of displacement. (**e**) Map view of the projection onto a horizontal plane of the (x,y) components of the displacement of the nodes of the neutral surface.

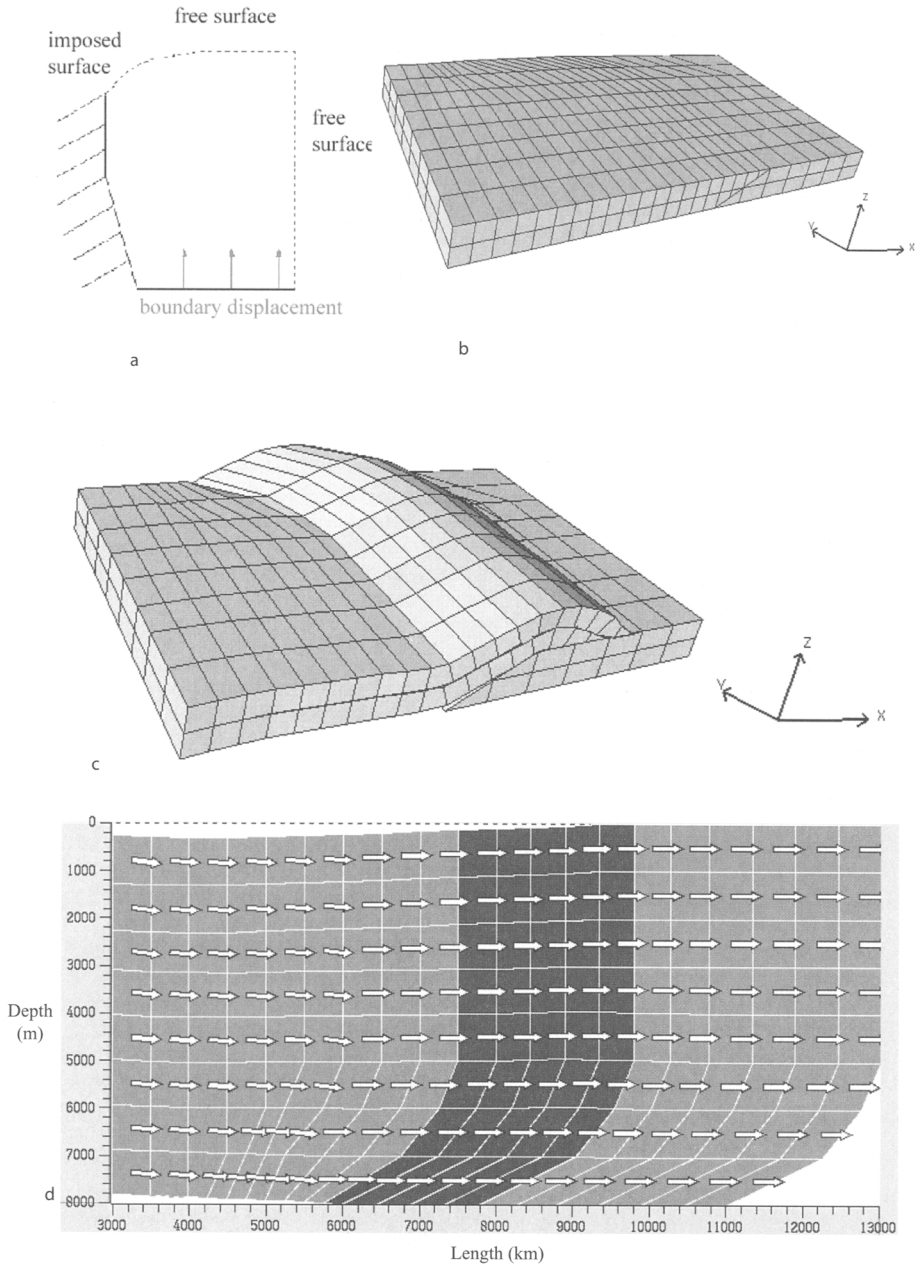

Fig. 4. Second 3D validation test: lateral boundary non-parallel to the boundary displacement. (**a**) Diagram of the boundary conditions. (**b**) Initial state of the block. (**c**) Deformed configuration after 3000 m of displacement. (**d**) Map view of the projection onto a horizontal plane of the (x, y) components of the displacement of the nodes of the neutral surface.

initial step (Fig. 3c) is 20 km long, 10 km wide and has a thickness of 1 km. The boundary condition is simple: we push at the back of the hanging wall, and we impose a 1 km displacement for each increment of time.

After 3 km of displacement, the basin presents a shape with a coherent geometry, and the edges, which are normal to the sliding support, show that we have a good flexural slip mechanism (Fig. 3d). If we look at the map in Figure 3e, which shows

the (x, y) component of the displacement of the nodes of the neutral surface, we see all displacement vectors are parallel to the imposed surface, which we can also find in a 2.5D model. Nevertheless, a glance at the edges on the imposed border shows 3D rigid rotations, with lateral components due to the curvature of the ramp. So the decomposition of the displacement is in two steps: (1) motion of the neutral surface, (2) rebuilding of the edges with rigid rotations around the neutral surface. It allows 3D deformation even if the displacement is parallel.

For the second test case, the ramp is the same (Fig 3b), but the imposed lateral border has a 5° angle with the displacement boundary (Fig. 4a, b). This geometry is truly 3D and cannot be described by a 2.5D approach. The boundary condition is still simple: we impose a displacement of 1 km at the back of the hanging wall. After 3 km of displacement (three time steps), we observe a deformation that is geometrically coherent, and we notice that the width of the hanging wall is well preserved (Fig. 4c). This is the first indication of the deformation. The second, and most significant, is shown on the map of the component of the displacement of the neutral surface nodes: the components are not parallel and have variations in all space directions (Fig. 4d).

The kinematic model used here to deform the basin has no constraint on volume variation. In fact, the choice of a constant volume is a very strong assumption that is very difficult to realize with a direct algorithm. We have chosen to work with the neutral surface of each layer and tried to preserve it instead of volume. Nevertheless, if we do not have the conservation of the volume as a main constraint, we need at least to control its variations to verify that the results are not unrealistic. Table 1 presents the global volume variation of the hanging wall throughout deformation. The variations remain low and fully acceptable.

Still, we can observe a few volume variations, which are due to compression and elongation at the hinge ramp. Such volume changes are related to various parameters, the initial geometry of the layers and the fault surfaces being one of the most important. However, for computatur limitation, it is not possible to reproduce exactly the natural geometry of the natural structures. So from this point of view, the modelling remains a crude approximation of natural behaviour. Introducing a more smooth variation along the fault surface could decrease the volume change. This will be tested and improved if necessary.

Table 1. *Variation of volume (as a percentage) in the hanging wall between the initial and deformed state for each time step*

	*T*0	*T*1	*T*2	*T*3	*T*4
Test case with a parallel imposed surface	0	0.85	0.97	1.43	0.57
Test non-parallel imposed surface	0	0.61	1.63	1.80	1.34

Several authors have pointed out the interest of introducing strain data in the balancing process (Woodward *et al.* 1986; Mitra 1994; Mac Naught & Mitra 1996; Von Winterfeld & Oncken 1995). This is theoretically possible with a discrete method but we did not try to implement such a constraint.

The kinematic model presented here was developed to be inserted late into basin modelling codes, as the structural part of the modelling. It is clear that there is more than one mechanism of deformation in the tectonic history of a basin. At least we can imagine that each layer can deform with its own mechanism. As an example of the versatility of the modelling code, we propose a model with two mechanisms of deformation: the bottom layer deforms with flexural slip and the top layer with vertical shear (Fig. 5a, b).

Conclusion

The model described here represents the next step of recent work performed in basin modelling at IFP (Schneider & Wolf 2000; Schneider *et al.* 2000). It was built to introduce more complex kinematics in the structural part as motions along 3D faults and 3D flexural slip. The great simplicity of its assumptions can be easily understood and implemented.

The geometries that can be treated are fully 3D, and are not restricted to cylindrical structures with parallel direction of displacement or built with topologically equivalent sections. One of the main strengths of the model is its capacity to apply different mechanisms of deformation to each layer of the basin (flexural slip, simple shear), and the layers are independent and treated individually. Another interesting point is the reversibility of the algorithm, which was one of the main goals to be achieved because it is to be inserted in a basin modelling code.

In the future, we now have to test the model on a real geological case, to see if the model is coherent with natural structures. This work will be of great help to pursue the study on internal deformations that take place in a layer throughout its deformation history.

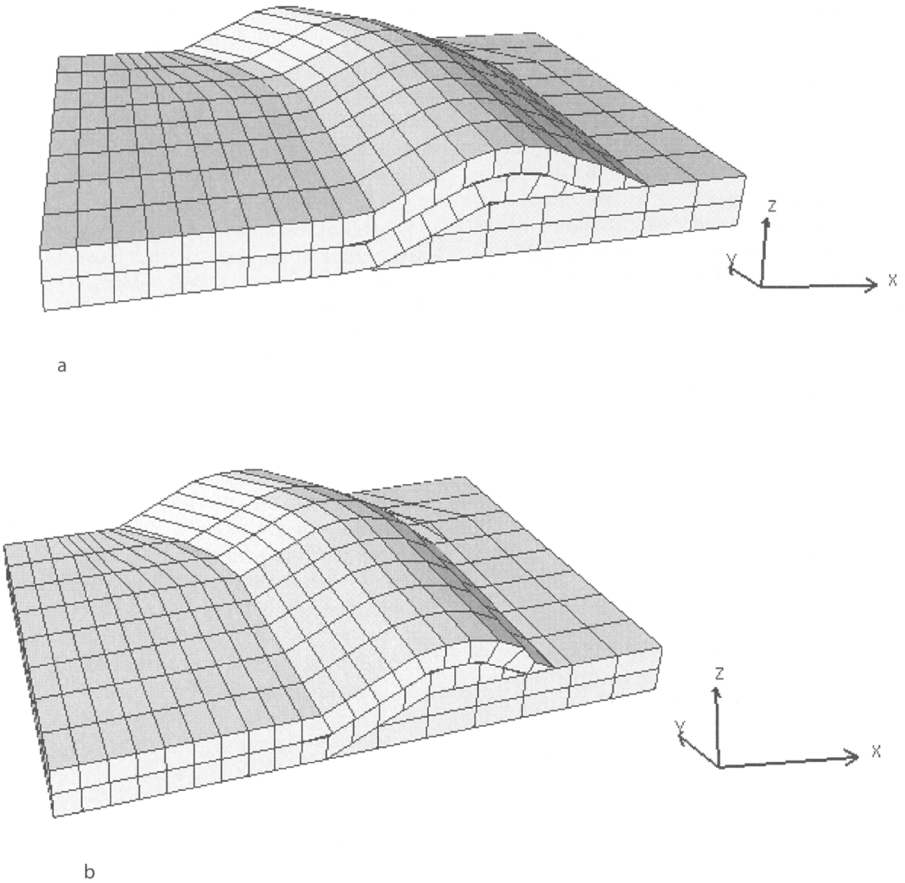

Fig. 5. Deformed basin, with combined flexural slip and vertical shear. (**a**) Flexural slip for the first layer and vertical shear for the second one. (**b**)Vertical shear for the first layer and flexural slip for the second one.

References

BARNICHON, J. D. 1998. *Finite element modelling in structural and petroleum geology*. PhD thesis, Université de Liège.

BENNIS, C., VEZIEN, J. G. & IGLESIAS, G. 1991. Piecewise surface flattening for non-distorted texture mapping. *Computer Graphics,* **25(4)**, 237–246.

CONTRERAS, J. & SUTER, M. 1990. Kinematic modelling of cross-sectional deformation sequences by computer simulation. *Journal of Geophysical Research,* **95**, 21913–21929.

CUNDALL, P. A. 1988. Formulation of a three-dimensional distinct element model-part I. A scheme to detect and represent contacts in a system composed of many polyhedral blocks. *International Journal of Rock Mechanics, Mineral Science & Geomechanical Abstracts,* **25(3)**, 107–116.

DAHLSTROM, C. D. A. 1969. Balanced cross sections. *Canadian Journal of Earth Sciences,* **6**, 743–757.

DE PAOR, D. G. 1988a. Balanced section in thrust belts, Part 1: construction. *AAPG Bulletin,* **72(1)**, 73–90.

DE PAOR, D. G. 1988b. Balanced section in thrust belts, Part 2: computerised line and area balancing. *Geobyte*, May, 33–37.

DIVIÈS, R. 1997. *FOLDIS: un modèle cinématique de bassins sédimentaires par éléments discrets associant plis, failles, érosion/sédimentation et compaction*. PhD thesis, Université Joseph Fourier de Grenoble.

EGAN, S. S., KANE, S., BUDDIN, T. S., WILLIAMS, G. D. & HODGETTS, D. 1999. Computer modelling and visualisation of the structural deformation caused by movement along geological faults. *Computers and Geosciences,* **25**, 283–297.

GRATIER, J. P. & GUILLIER, B. 1993. Compatibility constraints on folded and faulted strata and calculation of total displacement using computational restoration (UNFOLD program). *Journal of Structural Geology,* **15(3–5)**, 391–402.

GRATIER, J. P., GUILLIER, B., DELORME, A. & ODONNE, F. 1991. Restoration and balance of a folded and faulted surface by best-fitting of finite elements: principles and applications. *Journal of Structural Geology,* **13(1)**, 111–115.

HART, R., CUNDALL, P. A. & LEMOS, J. 1988. Formulation of a three dimensional distinct element model-part II. Mechanical calculations for motion and interaction of a system composed of many polyhedral blocks. *International Journal of Rock Mechanics, Mineral Science & Geomechanical Abstracts,* **25(3)**, 117–125.

HASSANI, R. 1994. *Modélisation numérique de la déformation des systèmes géologiques.* PhD thesis, Université de Montpellier II.

LAMOUREUX-VAR, V. 1997. *Modélisation de la compaction dans les bassins sédimentaires approche mécanique.* PhD thesis, Ecole polytechnique, Palaiseau.

MAC NAUGHT, M. A. & MITRA, G. 1996. The use of finite strain data in constructing a retrodeformable cross-section of the Meade thrust sheet, southeastern Idaho, U.S.A. *Journal of Structural Geology,* **18(5)**, 573–583.

MITRA, G. 1994. Strain variation in thrust sheets across the Sevier fold-and-thrust-belt (Idaho-Utah-Wyoming): implications for sections restoration and wedge taper evolution. *Journal of Structural Geology,* **16(4)**, 585–602.

NIÑO, F., CHÉRY, J. & GRATIER, J. P. 1998. Mechanical modelling of the Ventura basin: origin of the San Cayetano thrust fault and interaction with the Oak Ridge fault. *Tectonics,* **17**, 955–972.

RAMSAY, J. G. & HUBER, M. I. 1987. *The Techniques of Modern Structural Geology – Volume 2: Folds and Fractures.* Academic Press, New York.

SCHNEIDER, F. & WOLF, S. 2000. Quantitative HC potentiel evaluation using 3D basin modelling: application to Franklin structure, central graben, North sea, U.K. *Marine and Petroleum Geology.*

SCHNEIDER, F., POTDEVIN, J. L. & WOLF, S. 1996. Mechanical and chemical compaction model for sedimentary basin simulators. *Tectonophysics,* **263**, 307–317.

SCHNEIDER, F., WOLF, S., FAILLE, I. & POT, D. 2000. Un modèle de bassin 3D pour l'évaluation du potentiel pétrolier: application à l'offshore congolais. *Oil and Gas Science and Technology.*

SHAW, J. H., HOOK, S. C. & SUPPE, J. 1994. Structural trend analysis by axial surface mapping. *AAPG Bulletin,* **78**, 700–721.

SUPPE, J. 1983. Geometry and kinematic of fault-bend folding. *American Journal of Science,* **283**, 684–721.

VON WINTERFELD, C. & ONCKEN, O. 1995. Non-plane strain in section balancing: calculation of restoration parameters. *Journal of Structural Geology,* **17(3)**, 457–450.

WALTHAM, D. 1989. Finite difference modelling of hanging wall deformation. *Journal of Structural Geology,* **11**, 433–437.

WALTHAM, D. 1990. Finite difference modelling of sandbox analogues, compaction and detachment free deformation. *Journal of Structural Geology,* **12**, 375–381.

WILKERSON, M. S. & MEDWEDEFF, D. A. 1991. Geometrical modelling of fault-related folds: a pseudo-three-dimensional approach. *Journal of Structural Geology,* **13**, 801–812.

WOODWARD, N. B., GRAY, D. R. & SPEAR, D. B. 1986. Including strain data in balanced cross section. *Journal of Structural Geology,* **8(3–4)**, 313–324.

ZOETEMEIJER, R. 1992. *Tectonic modelling of forelands basins, thin skinned thrusting, syntectonic sedimentation and lithospheric flexure.* PhD thesis, Vrije Universiteit Amsterdam.